Coastal Wind-Driven Circulation in the Vicinity of a Bank. Part II: Modeling Flow over the Heceta Bank Complex on the Oregon Coast

MICHAEL M. WHITNEY

Department of Marine Sciences, University of Connecticut, Groton, Connecticut

J. S. ALLEN

College of Oceanic and Atmospheric Sciences, Oregon State University, Corvallis, Oregon

(Manuscript received 11 December 2007, in final form 7 November 2008)

ABSTRACT

This study investigates wind-driven circulation in the vicinity of the Heceta Bank complex along the Oregon shelf. Numerical experiments forced with steady winds (0.1 Pa) are conducted; upwelling and downwelling cases are compared. The asymmetric bank bathymetry is the only configurational difference from the symmetric bank runs analyzed in Part I (Whitney and Allen). Upwelling-favorable winds generate an upwelling front and southward baroclinic jet. Model results indicate the upwelling jet is centered on the 100-m isobath along the straight shelf. The jet follows this isobath offshore around the northern part of the bank but separates from sharply turning isobaths in the southern half and flows over deeper waters. The jet turns back toward the coast farther downstream. Inshore of the main jet, currents reverse and flow back onto the bank. These reversed currents turn southward again (at the bank center) and join a secondary southward coastal upwelling jet. This secondary coastal jet converges with the stronger main jet farther downstream. Upwelling is intense at the northern bank edge near the coast, where a dense water tongue is advected over the bank. Upwelling also is strong on the southern bank half where the flow turns and reverses. Other areas of the bank have reduced upwelling or even downwelling during upwelling-favorable winds. Downwelling-favorable winds drive a near-bottom density front and a northward jet. The slower downwelling jet flows along the 130-m isobath over the straight shelf. The jet departs from isobaths over the southern bank half and follows a straighter path over shallower waters. There are no reversed currents over the bank. The bank is an area of reduced downwelling. Some of the differences in the evolution of the current and density fields are linked to fundamental differences between the upwelling and downwelling regimes; these are anticipated by the symmetric bank results of Part I. Other differences arise because of the bank asymmetry and opposite flow directions over the bank.

The lowest-order depth-averaged across-stream momentum balance remains geostrophic over the bank. Advection, ageostrophic pressure gradients, wind stress, and bottom stress all are important in the depth-averaged alongstream momentum balance over the Heceta Bank complex. Both across-shelf and alongshelf density advection are important. Barotropic potential vorticity is not conserved over the bank, but the tendency for relative vorticity changes and depth changes to partially counter each other influences the different paths of the upwelling and downwelling jets. There are several regions of active upwelling and downwelling over the bank. In these areas, vertical velocities at the top of the bottom boundary layer are linked to topographic upwelling and downwelling and Ekman pumping. There is considerable spatial variability in the currents, densities, and dynamics over the Heceta Bank complex.

1. Introduction

This study investigates the effects banks have on wind-driven coastal upwelling and downwelling along stratified continental shelves. Whitney and Allen (2009, hereafter Part I) analyze numerical experiments for upwelling and downwelling over symmetric idealized banks. Results indicate significant alongshelf variability over the bank and pronounced differences between the upwelling and downwelling regimes. This part of the study (Part II) conducts similar experiments for the Heceta Bank complex on the Oregon continental shelf (Fig. 1); this feature extends about 175 km alongshore,

Corresponding author address: Michael M. Whitney, Department of Marine Sciences, University of Connecticut, 1080 Shennecossett Road, Groton, CT 06340-6097.
E-mail: michael.whitney@uconn.edu

DOI: 10.1175/2008JPO3967.1

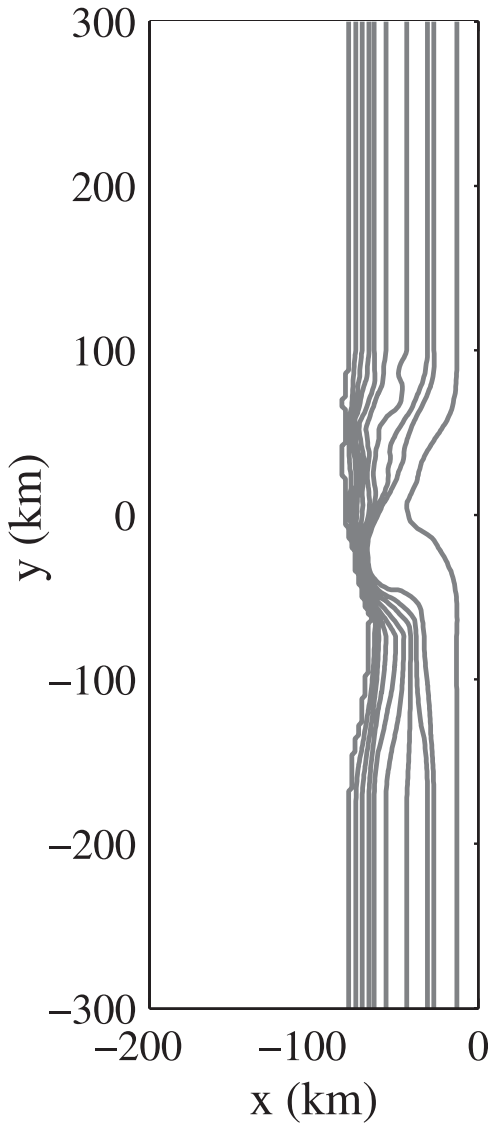

FIG. 1. Model domain and bathymetry. The bathymetry along the straight shelf is representative of the Oregon continental shelf (following the shelf section at 45°N). The bank bathymetry is a smoothed version (with a 25-km square filter window) of the Heceta Bank complex bathymetry. The coast is on the right side of the domain. The gray lines are isobaths contoured at a 100-m interval beginning with the 100-m isobath and ending with the 1000-m isobath.

widens the shelf, and includes the Heceta, Perpetua, and Stonewall Banks. The standard bank studied in Part I has similar dimensions to the Heceta Bank complex. The wind forcing and initial conditions are kept the same as Part I. Upwelling and downwelling dynamics over the Heceta Bank complex are expected to exhibit similarities to the standard symmetric bank results analyzed and discussed in Part I. The alongshelf asymmetry of the Heceta Bank complex bathymetry, however, can cause significant differences. The tightly curved isobaths on the south side of the bank may cause pronounced flow separation from isobaths.

Wind-driven flow in the vicinity of the Heceta Bank complex has been observed and previously modeled. The most recent study is the Coastal Ocean Advances in Shelf Transport (COAST) project funded by the National Science Foundation. Intensive field efforts observed the prevailing upwelling conditions during summer 2001 and downwelling conditions during winter 2003. Barth et al. (2005) and Kosro (2005) report that the southward upwelling jet is strongly affected by shelf bathymetry. The core of the observed jet is located over bottom depths of 80–100 m. The summer upwelling jet approximately follows these isobaths and deflects offshore along the north side of the bank. Both papers document the weak flow region shoreward of the jet. A secondary jet has been observed at the coast over the bank. This inshore jet forms because of local upwelling over the bank (Barth et al. 2005). The stronger offshore jet overshoots isobaths at the south side of the bank and flows over deeper waters (Castelao and Barth 2006). There is a wide region of upwelled water inshore of the main jet over the bank (Barth et al. 2005). Previous simulations of upwelling conditions show the offshore deflection of the baroclinic jet, the development of the secondary coastal jet, and the wide region of upwelled water over the Heceta Bank complex (Oke et al. 2002; Kurapov et al. 2005; Gan and Allen 2005). These simulation efforts demonstrate the importance of bottom stress and ageostrophic pressure gradients over the bank. Observations during winter downwelling conditions reveal a northward downwelling jet that is influenced by alongshelf variations in shelf bathymetry; however, it does not deflect offshore like the summer upwelling jet (P. M. Kosro 2005, personal communication). The winter 2003 COAST study period is the focus of continued analysis. A realistic modeling simulation of the downwelling conditions during this period will be the subject of a future study.

The previous simulations were forced with realistic time-varying winds and included bathymetry representative of the entire Oregon shelf. The present effort conducts numerical experiments with steady winds and includes only the alongshelf variations in bathymetry introduced by the Heceta Bank complex. In this way, the dynamical effects of the bank can be isolated and analyzed. The present effort compares the flow regimes that develop in response to sustained upwelling-favorable and downwelling-favorable winds. Much less is known about dynamics during downwelling conditions; the Part I results indicate there are interesting similarities and fundamental differences between upwelling

and downwelling over banks. The Part II experiments build on the insight gained from the symmetric bank runs studied in Part I. This paper utilizes the symbols defined and equations written in Part I. The next section of this paper discusses the model setup for the Heceta Bank runs. Section 3 describes the density and current fields that develop during upwelling and downwelling conditions. The dynamics are discussed in section 4; the momentum balances, density balances, and vertical velocity contributions are analyzed. The final section includes a summary and conclusions.

2. Model configuration

The numerical experiments are carried out using the Regional Ocean Modeling System (ROMS, version 2.1); the governing equations and differencing schemes are discussed in Haidvogel et al. (2000) and in Shchepetkin and McWilliams (2005). The primary model settings, time steps, and boundary conditions are the same as in Part I. The model domain (Fig. 1) has the same dimensions (200 × 600 km) and resolution (2-km cells with 40 *s*-coordinate levels). The only configurational difference from Part I is the bathymetry.

A straight coast borders the eastern side of the periodic model domain. To isolate the effects of the Heceta Bank complex, the model bathymetry is uniform alongshelf except near the bank. The bank bathymetry is a smoothed version (with a 25-km square filter window) of the Heceta Bank complex (Fig. 1). The bathymetry along the straight shelf matches the bathymetry on the northern end of the bank (at 45°N). The bank complex is 150 km long. The 200-m isobath curves out to 40 km farther offshore (70 km from the coast) over the bank. The 1000-m isobath remains essentially straight. Unlike the idealized banks studied in Part I, Heceta Bank complex is asymmetric. The maximum offshore excursion of the 200-m isobath is located farther south than the crest of the 100-m isobath. The radius of curvature of the 200-m isobath (r_b) is approximately 60 km along the north side and only 10–20 km over the south side.

The model is initialized from rest with a constant buoyancy frequency of 10^{-2} s^{-1}. The slope Burger number is order one and the internal deformation radius is 10 km for height $h = 100$ m. As in Part I, the model is forced with steady spatially uniform alongshelf wind stress ($\tau^{sy} = \pm 0.1$ Pa). Subinertial results (averaged over a 17-h period) from day 10 are discussed in this paper.

Four numerical experiments are described in this part of the study. The two primary cases are for the Northern Hemisphere (44.5°N latitude, $f = 1.022 \times 10^{-4}$ s^{-1}): the upwelling case has southward winds ($\tau^{sy} < 0$) and the downwelling case has northward winds ($\tau^{sy} > 0$). Since the Heceta Bank complex is asymmetric (unlike the symmetric banks studied in Part I), the dynamics should depend on the flow direction over the bank. To document these differences, two so-called Southern Hemisphere cases ($f = -1.022 \times 10^{-4}$ s^{-1}) are run that are not realized in nature for the Heceta Bank complex: the upwelling case has northward winds ($\tau^{sy} > 0$) and the downwelling case has southward winds ($\tau^{sy} < 0$). These four cases help determine which effects are related to the bank asymmetry and which are linked to fundamental differences in upwelling and downwelling dynamics.

3. Results

The velocity and density fields that develop over the Heceta Bank complex during upwelling and downwelling are described in this section. The discussion focuses on the Northern Hemisphere upwelling ($f > 0$, $\tau^{sy} < 0$) and downwelling ($f > 0$, $\tau^{sy} > 0$) cases. The hypothetical Southern Hemisphere upwelling ($f < 0$, $\tau^{sy} > 0$) and downwelling ($f < 0$, $\tau^{sy} < 0$) cases are included as a contrast to the Northern Hemisphere runs.

a. Northern Hemisphere upwelling case

By day 10 (Fig. 2a), the upwelling jet is 30 km wide with a 60 cm s^{-1} depth-averaged core velocity. The jet follows the 100-m isobath offshore over the northern half of the bank. This jet overshoots the bathymetry where isobaths turn sharply over the southern bank; it moves over deeper waters after separating from isobaths. Streamlines indicate that the jet slows and widens over the deeper waters, turns back toward shore, and reattaches to the coast downstream of the bank. Inshore of the main jet there is a low-velocity region where the current reverses. The transport streamlines indicate that the reversed flow turns anticyclonically at the bank center and joins the southward flow along the coast as in the symmetric case of Part I. This secondary coastal jet is associated with a second density front produced by local upwelling over the bank. This structure of the currents is consistent with observations (e.g., Kosro 2005). The secondary coastal jet and stronger main jet converge farther downstream. The most significant difference from Part I is the degree of streamline separation from isobaths over the downstream half of the Heceta Bank complex.

As in Part I, a dense water tongue has been advected over the northern half of the bank (Fig. 3a). In spite of the upwelling-favorable conditions, the bank has areas of low-density water near the coast and on its offshore edge. Along the straight shelf, bottom density has increased most along the coastal upwelling front (Fig. 4a).

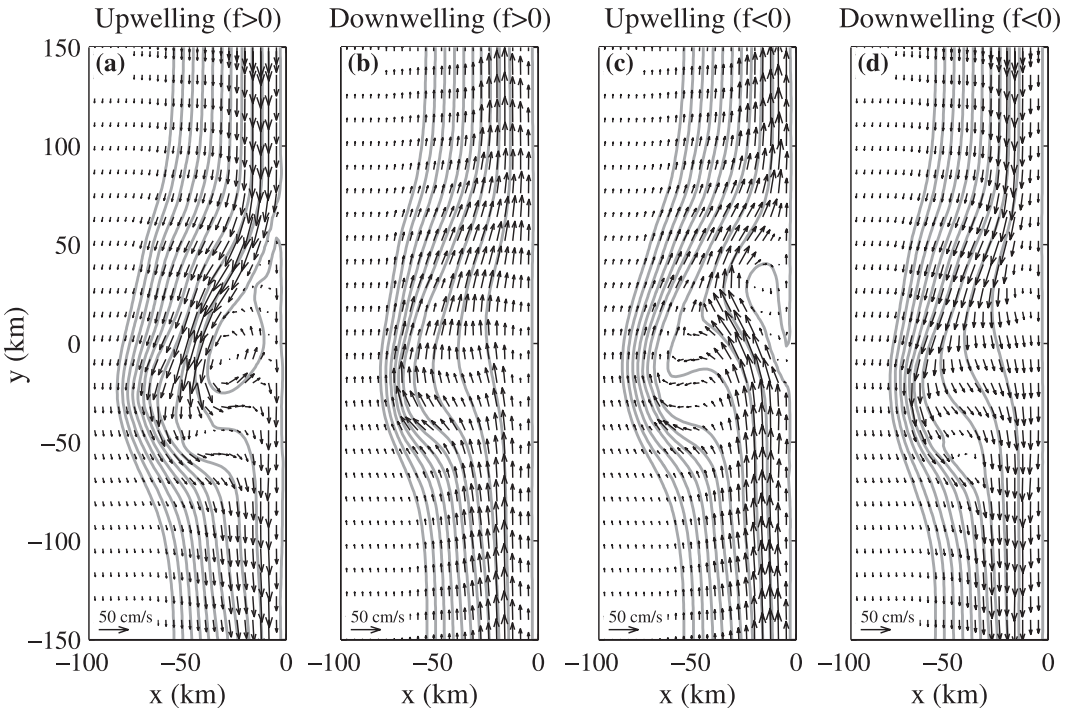

FIG. 2. Depth-averaged velocity vectors and transport streamlines on day 10 during (a) upwelling and (b) downwelling for the Northern Hemisphere ($f > 0$) runs and during (c) upwelling and (d) downwelling for the hypothetical Southern Hemisphere runs ($f < 0$).

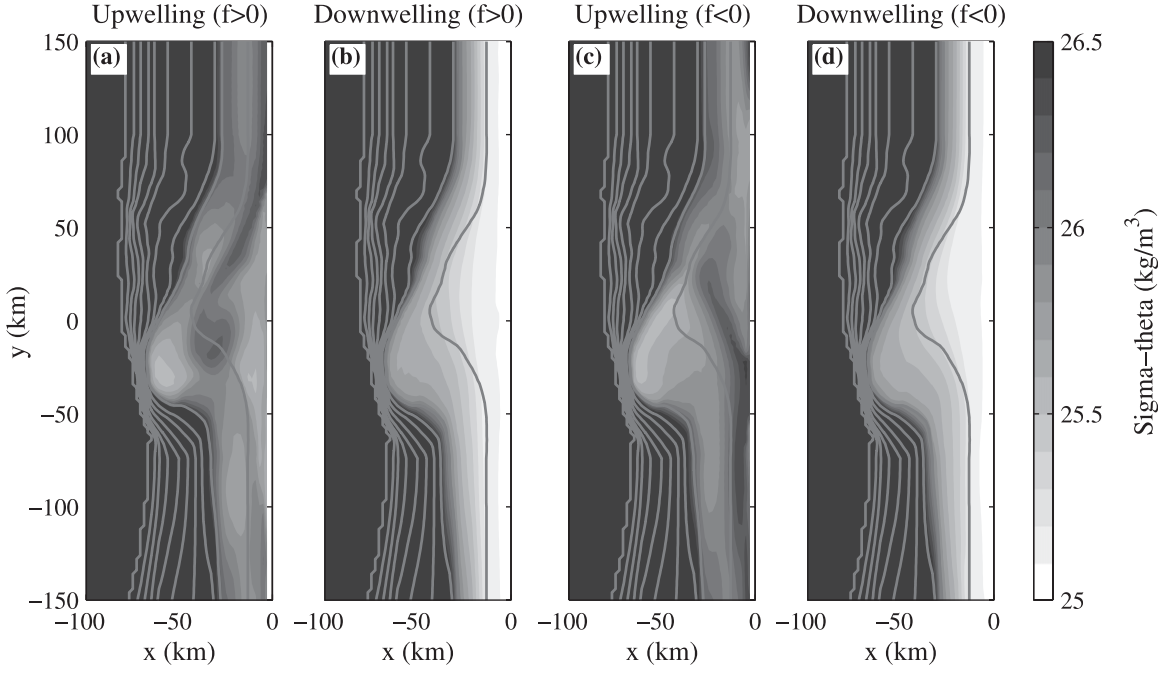

FIG. 3. Depth-averaged density field on day 10 during (a) upwelling and (b) downwelling for the Northern Hemisphere ($f > 0$) runs and during (c) upwelling and (d) downwelling for the hypothetical Southern Hemisphere runs ($f < 0$). Gray lines indicate isobaths, contoured at a 100-m interval.

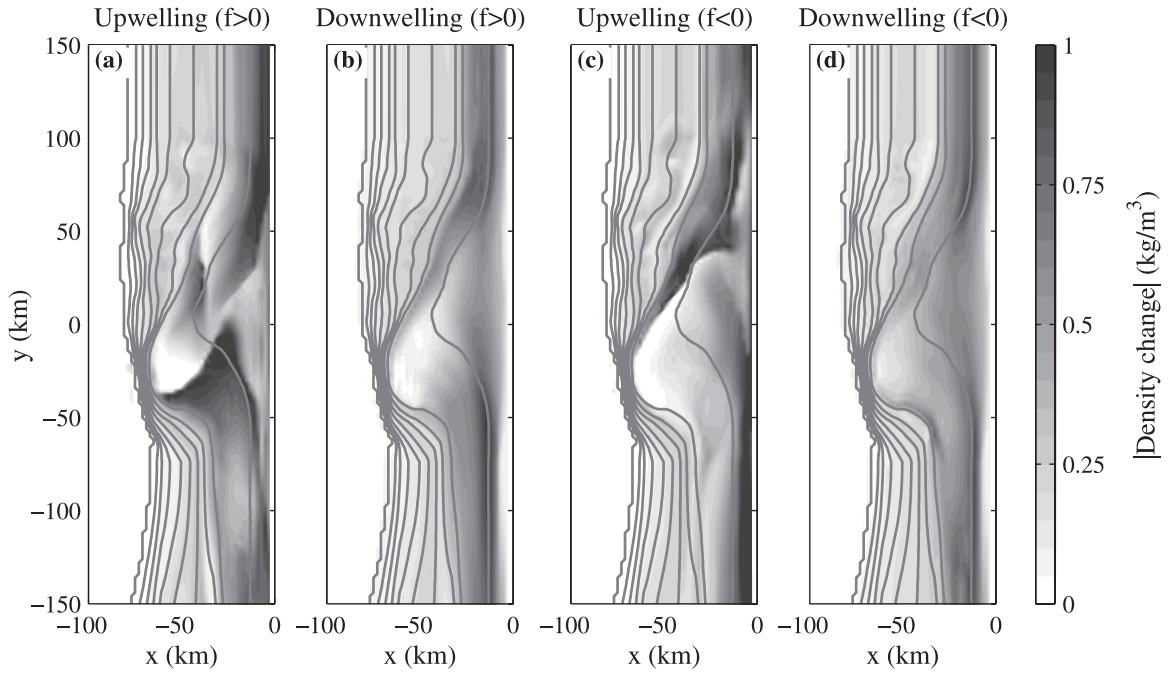

FIG. 4. Bottom density change (day 10) during (a) upwelling and (b) downwelling for the Northern Hemisphere ($f > 0$) runs and during (c) upwelling and (d) downwelling for the hypothetical Southern Hemisphere ($f < 0$) runs. Density increases in the upwelling cases and decreases in the downwelling cases. Gray lines indicate isobaths that are contoured at a 100-m interval.

Bottom density increases are large at the upstream edge of the bank (as in Part I). Upwelling is intensified here because the jet shoals upon first encountering the bank. This shoaling lifts denser waters that then are brought to the surface by the local across-shelf upwelling circulation. Over the northern half of the bank, bottom densities have increased over the wide region inshore of the main jet. There is a smaller isolated area of density increase between the 100- and 200-m isobaths near the bank center. Over the southern part of the bank, there is a roughly triangular region of larger bottom density increases. This area originated where the 200-m isobath is nearly perpendicular to the coast. It intensified and expanded northward and inshore as the upwelling conditions continued over 10 days. There are large areas of the bank with little bottom density change; these are located near the coast and at the offshore edge.

These results are similar to the standard symmetric bank run (Part I) in many ways: the main jet moves offshore over the bank, currents reverse inshore of the jet, upwelling is intense at the upstream bank edge, and upwelling is reduced over some other bank sections. The most pronounced differences occur over the southern bank half. In the Heceta Bank case, the main jet separates from isobaths and flows into much deeper water. The current reversal inshore of this jet occurs over deeper waters. As the reversed currents shoal, they lift dense waters from depth. This advection of dense waters leads to pronounced upwelling over the southern part of the bank; the upwelling is stronger than over the southern half of the symmetric bank.

The jet relative vorticity (Fig. 5a) is the same scale as f. The shoreward side of the jet has a narrower shear zone (with intense cyclonic vorticity) than the wide lateral shear zone along the seaward side (with weaker anticyclonic relative vorticity). The maximum curvature vorticity magnitude (Fig. 6a) is $0.3f$, indicating that the lowest-order across-stream momentum balance does not involve advection. The negative curvature vorticity at the upstream edge is associated with the offshore deflection (anticyclonic turning) of the jet. Areas of strong positive curvature vorticity (cyclonic turning) are associated with the jet turning back toward the coast and with the reversed current. There is strong negative curvature over the southern part of the bank, where the flow turns (anticyclonically) and realigns itself with the coast.

The Part I results indicate the upwelling jet does not follow isobaths where the isobath radius of curvature is less than the inertial radius ($V/fr_b \leq 1$). The degree of flow separation for banks with such tightly turning isobaths is significantly larger than over banks with less curved isobaths. Over the Heceta Bank complex, the flow follows isobaths over the northern part of the bank,

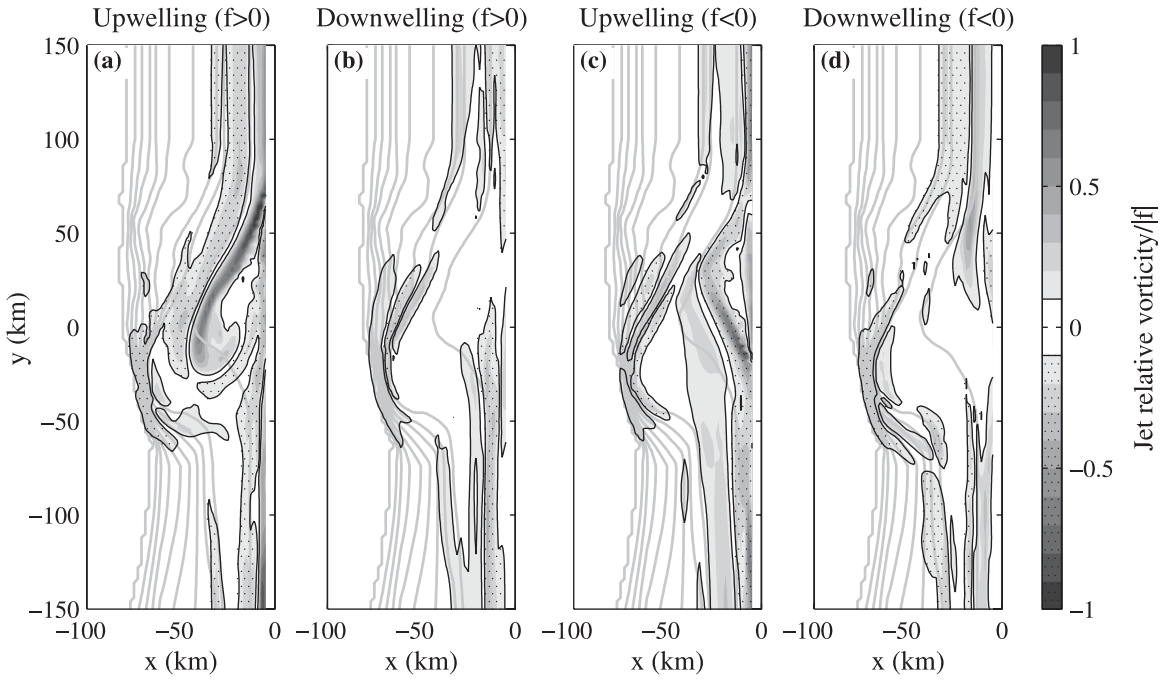

FIG. 5. Jet relative vorticity of the depth-averaged flow ($-\partial V/\partial n$) scaled by $|f|$ during (a) upwelling and (b) downwelling for the Northern Hemisphere ($f > 0$) runs and during (c) upwelling and (d) downwelling for the Southern Hemisphere ($f < 0$) runs. Isobaths are shown as in Fig. 4.

where isobath curvature is gentle; the average r_b is 60 km and the minimum r_b is 30 km. The maximum Rossby number for a 60 cm s^{-1} flow following isobaths over the northern section is 0.2. Isobaths turn sharply over the southern part of the bank; the minimum r_b is 8 km. The maximum Rossby number necessary for a 60 cm s^{-1} flow to follow isobaths around the southern bank section is 0.7. This value is more than double the maximum Ro (Fig. 6a) and is near the threshold value ($V/fr_b \approx 1$) for pronounced flow separation. One effect of the bank asymmetry is that the main jet separates from isobaths over the southern part of the bank; there was no similar overshoot over the standard symmetric bank in Part I.

Cross sections of the velocity and density fields (Fig. 7) give information on the vertical structure of the circulation during upwelling-favorable winds. Results along the straight shelf follow classical two-dimensional (2D) upwelling dynamics (discussed in Part I). Over the bank the density field is modified extensively by the offshore deflection of the baroclinic jet, reversals of the alongshelf current, and changes in the across-shelf circulation. The main upwelling front and jet move offshore and advect dense water over the bank. Inshore of the dense water tongue, the across-shelf density gradient (and isopycnal slope) changes sign and is in thermal wind balance with the geostrophic northward flow. These features are similar to those seen over the symmetric bank modeled in Part I. Over the southern bank half, sections indicate two density fronts and two corresponding jets. The secondary coastal upwelling front and jet (because of local wind-driven upwelling over the bank) are weaker than the main front and jet farther offshore. At the southern edge of the bank, there is an area of strong near-bottom density increase without a corresponding surface signature. This upwelling is linked to the reversed (northward) currents that flow onto the bank, generating upslope near-bottom flow as they shoal. Isopycnals indicate an area of downwelling at the offshore edge of the southern bank section. This middepth downwelling is evident over the standard symmetric bank studied in Part I. Upward velocities (not shown) at the southern edge of the bank remove the signature of this downwelling farther downstream; there are no areas of net density decrease south of the bank. Downstream of the bank, the main jet returns to the coast (merging with the weaker secondary coastal jet) and the density field matches the 2D upwelling solution again.

b. Northern Hemisphere downwelling case

By day 10 (Figs. 2b and 3b) over the straight shelf, the downwelling jet is 30 km wide with a 50 cm s^{-1} depth-averaged core velocity centered on the 130-m isobath. The downwelling jet is slower than the upwelling jet and the bending around the bank is not as pronounced

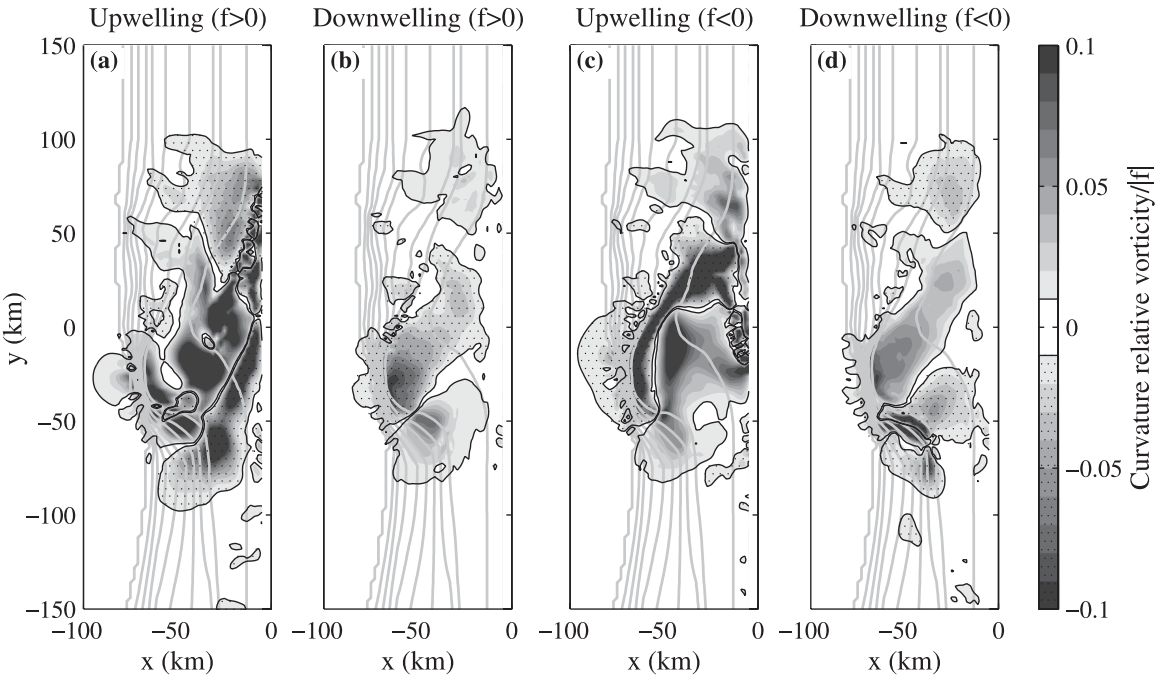

FIG. 6. Curvature relative vorticity of the depth-averaged flow (V/r) scaled by $|f|$ during (a) upwelling and (b) downwelling for the Northern Hemisphere ($f > 0$) runs and during (c) upwelling and (d) downwelling for the Southern Hemisphere ($f < 0$) runs. Isobaths are shown as in Fig. 4. The contour range is 10 times smaller than for Fig. 5.

as the offshore deflection of the upwelling jet. The core of the downwelling jet shoals over the bank. Unlike the upwelling case, there are no reversed currents (areas of southward flow) over the bank. These results are similar to the symmetric bank run (Part I). Local downwelling and density advection have decreased bottom densities (Fig. 4b). The largest density decreases are near the 100-m isobath over the straight shelf. As in Part I, the bank is an area of reduced downwelling. Bottom densities have decreased inshore of the 100-m isobath along the downwelling jet path. Bottom density also decreases over much of the offshore bank edge.

The relative vorticity of the depth-averaged flow highlights additional features of the downwelling circulation. The vorticity associated with the lateral shear of the jet (Fig. 5b) is strongest over the straight shelf, where the jet velocities are largest. The jet vorticity is not as large ($\pm 0.5f$) as in the upwelling case ($\pm f$) because the downwelling jet has lower core velocities. The depth-averaged curvature vorticity (Fig. 6b) ranges between $\pm 0.1f$; thus, the lowest-order depth-averaged across-stream momentum balance does not involve centrifugal acceleration. The strongest curvature occurs over the southern part of the bank. The downwelling jet has slower velocities and a smaller inertial radius than the upwelling jet; consequently, it should be able to follow more tightly turning isobaths. Flow following the sharply curved isobaths over the southern bank section (with minimum $r_b = 8$ km) would have a Rossby number of 0.6 for $V = 0.50$ cm s^{-1} and 0.3 for $V = 25$ cm s^{-1}; this is not as close to the flow separation threshold as the upwelling case. Nevertheless, the flow does not turn as tightly as isobaths over the southern bank section. The core of the downwelling jet departs from isobaths over the bank; the jet takes a straighter path into shallower waters. The flow more closely follows isobaths over the gently curving northern bank section.

Cross sections (Fig. 8) show the vertical structure of the downwelling circulation. Dynamics over the straight shelf are consistent with 2D downwelling circulation (discussed in Part I). The density front, downwelling jet, and across-shelf circulation are modified over the bank. As discussed, the front and jet move offshore over the southern bank section and move back onshore over the northern half. The across-shelf density gradient and jet velocity are weakest over the bank. The water inshore of the density front is vertically well mixed; the inshore density now equals the surface density. The across-shelf density gradient approaches zero inshore of the downwelling front. Vertical velocities (not shown) indicate the presence of bottom boundary layer instabilities similar to those described in Allen and Newberger (1998), except that these instabilities exhibit alongshelf variability. Positive vertical velocities (not shown) upwell

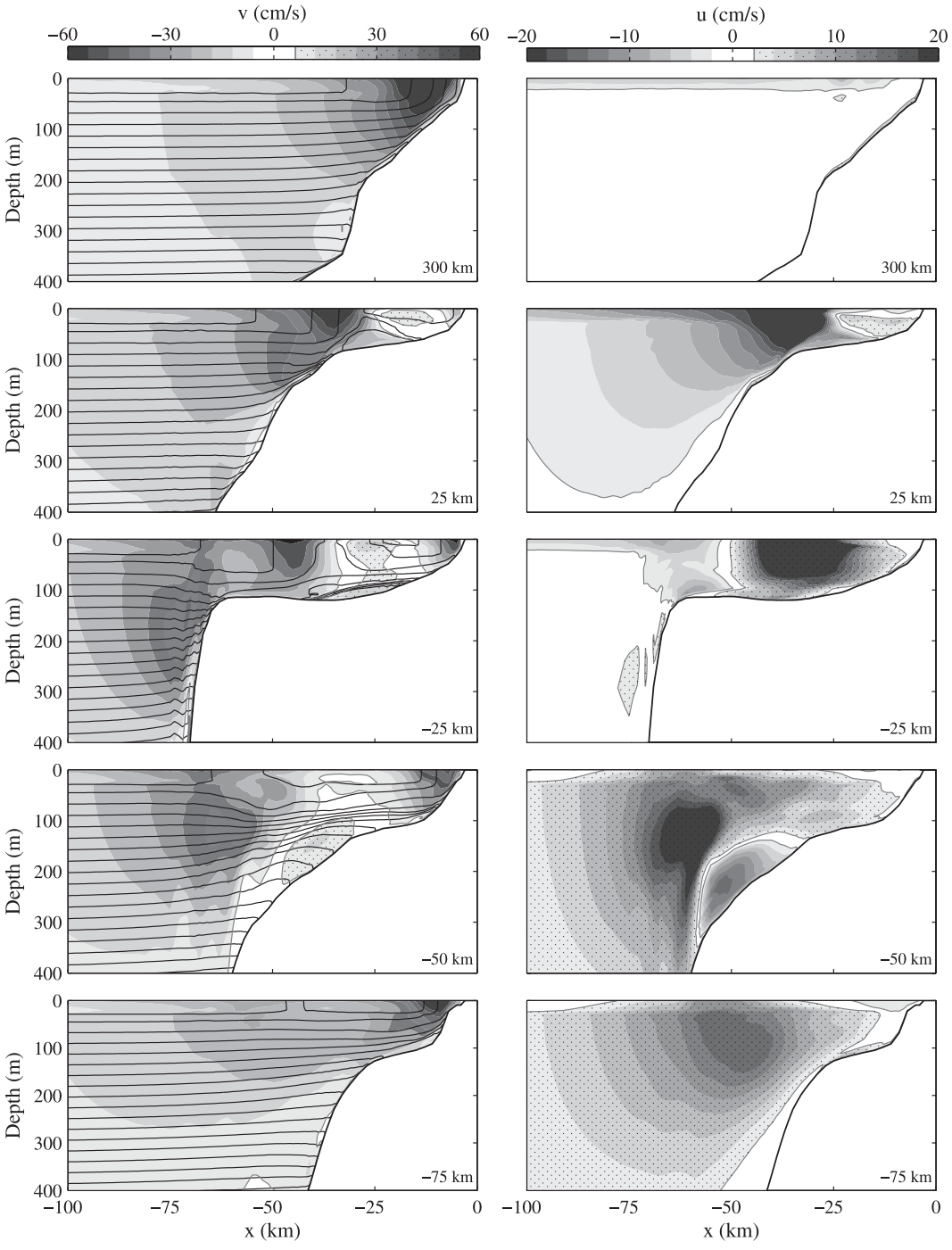

FIG. 7. Cross sections during the Northern Hemisphere upwelling run (day 10). (top row) Results on the straight shelf (y = 300 km). (bottom rows) The sequence southward (downstream) over the bank. Alongshelf velocity (positive northward) and across-shelf velocity (positive onshore) are contoured. (left) Isopycnals are line contoured (0.25 kg m^{-3} interval).

isopycnals at middepth along the offshore edge over the southern bank section ($y = -25$ km section). This localized upwelling is linked to the shoaling of the flow over the bank. Negative vertical velocities (not shown) restore isopycnals to a downwelled state over the northern part of the bank. The downwelling front and jet return to the coast downstream of the bank, where circulation again is governed by 2D downwelling dynamics.

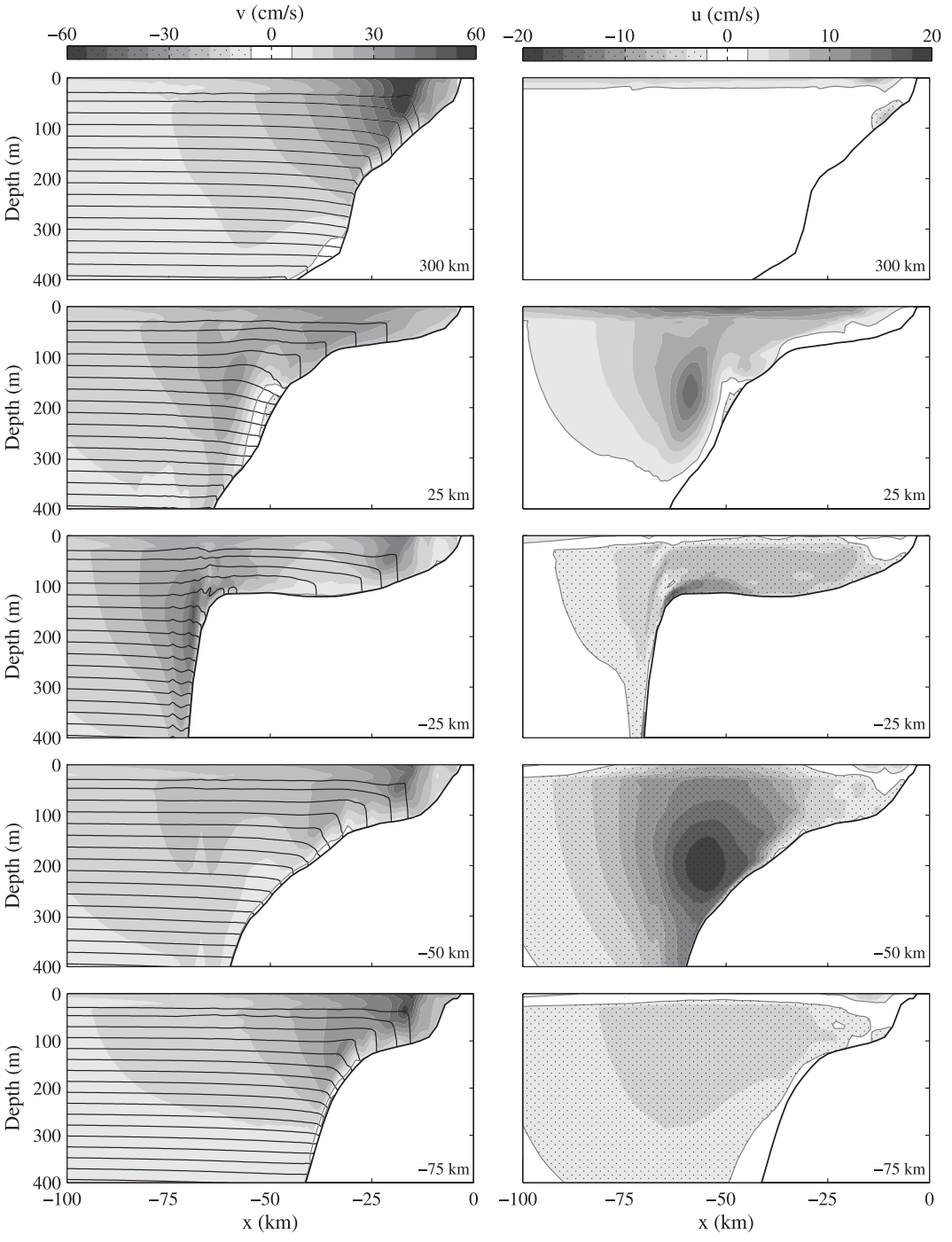

FIG. 8. Cross sections during the Northern Hemisphere downwelling run (day 10). The panels are arranged as in Fig. 7. (top row) The straight shelf; (bottom rows) the sequence southward (upstream) over the bank.

There are conspicuous differences between upwelling and downwelling results for the standard symmetric bank (Part I). These differences are intensified over the asymmetric bathymetry of the Heceta Bank complex. The Heceta Bank complex, unlike the standard symmetric bank, has sharply turning isobaths over its southern side. The upwelling jet separates from these tightly curved isobaths over the downstream bank section and flows over much deeper waters. The upwelling jet then turns back toward the coast and rejoins the initial

isobath farther downstream. In contrast the downwelling jet approaches the sharply turning isobaths over the upstream section of the bank and shoals over the bank.

c. Southern Hemisphere cases

The Southern Hemisphere cases have been run to investigate the consequences of reversing the primary flow direction without switching between an upwelling and downwelling regime. These purely hypothetical cases are useful in isolating the effects of bank asymmetry from differences between upwelling and downwelling conditions.

The depth-averaged density and velocity fields for the Southern Hemisphere upwelling case (Figs. 2c and 3c) are more similar to the other upwelling case than the Northern Hemisphere downwelling case: dense water is upwelled at the upstream (southern) bank edge, the upwelling jet advects dense waters over the bank, and there is a reversed current inshore of the dense water tongue. There are pronounced differences between the upwelling runs because of the asymmetric bathymetry. In the Southern Hemisphere case, the northward upwelling jet first encounters the sharply turning isobaths of the southern (upstream) bank section. The jet shoals after separating from isobaths. In contrast, the Northern Hemisphere upwelling jet flows into deeper waters after separating from isobaths over the downstream side. There are conspicuous differences in the bottom density change patterns (Figs. 4a and 4c) because of the opposite flow direction and different consequences of separation from isobaths. The relative vorticity associated with the lateral shear of the upwelling jet (Fig. 5c) is similar to the other upwelling case. The curvature relative vorticity has a similar magnitude; the strongest flow curvature is largest over the southern bank section for both cases (Fig. 6c). The flow curvature in the upwelling cases is stronger than in the downwelling cases because of the faster flow velocities and the increased offshore deflection. In all cases, the flow curvature remains small enough that centrifugal acceleration is not part of the lowest-order depth-averaged across-stream momentum balance.

The two downwelling cases are more similar than the two upwelling cases. The density and velocity fields for the hypothetical Southern Hemisphere downwelling case (Figs. 2d and 3d) share many features with the Northern Hemisphere downwelling case: depth-averaged density decreases toward shore, the downwelling jet shoals as it bends around the bank, flow is slowest over the bank, and there are no reversed currents. Streamlines follow similar paths in both cases, even though the flow is in the opposite direction. In both downwelling cases, the bank is an area of reduced downwelling; the bottom density change pattern (Fig. 4d) is similar to the Northern Hemisphere case. The relative vorticity fields also are similar: the lateral shear of the jet (Fig. 5d) and flow curvature (Fig. 6d) have magnitudes and spatial structure similar to the other downwelling case but with opposite sign.

The Southern Hemisphere downwelling and the Northern Hemisphere upwelling cases have the same flow direction but extremely different jet paths. The Southern Hemisphere upwelling and Northern Hemisphere downwelling cases also are quite different, despite having the same flow direction. Changing flow directions has the most pronounced affect on the two upwelling runs. Comparison of the four cases indicates that bank asymmetry does influence the flow patterns, but many differences in the current and density fields are related to the fundamentally different dynamics during upwelling and downwelling conditions.

d. Jet path and barotropic potential vorticity changes

The path of the Northern Hemisphere upwelling and downwelling jets (Fig. 9a) is tracked by following the transport streamline that originates in the jet core over the straight shelf. Depths along the jet core paths are shown in Fig. 9b. The upwelling jet originates on the 100-m isobath and oscillates around this isobath over the northern (upstream) side of the bank; the jet core is between the 87- and 102-m isobath over this section. After separating from the sharply turning isobaths of the southern side, the jet quickly flows over much deeper waters; the maximum depth is 217 m. This degree of isobath departure does not occur over the standard symmetric bank (Part I). The core of the downwelling jet is farther offshore than the upwelling jet over the straight shelf and closer to the coast over the bank. The downwelling jet shoals from the 130-m isobath to the 80-m isobath over the southern (upstream) part of the bank. The jet moves back toward deeper waters over the northern side and returns to its initial isobath farther downstream. The paths of the Southern Hemisphere jets are shown in Fig. 9c. The Southern Hemisphere upwelling jet shoals after separating from isobaths over the southern side of the bank; the jet position varies between the 86- and 124-m isobaths (Fig. 9d). The upwelling jet paths are different because the Southern Hemisphere upwelling jet encounters the tightly turning isobaths over the upstream side, while the Northern Hemisphere jet reaches these isobaths on the downstream side. The Southern Hemisphere downwelling jet follows a similar path to the Northern Hemisphere jet; the jet shoals from the 130-m isobath to the 84-m isobath over the bank. Because of the bank asymmetry, changing the flow direction changes the jet path; differences are strongest for the upwelling cases. Even

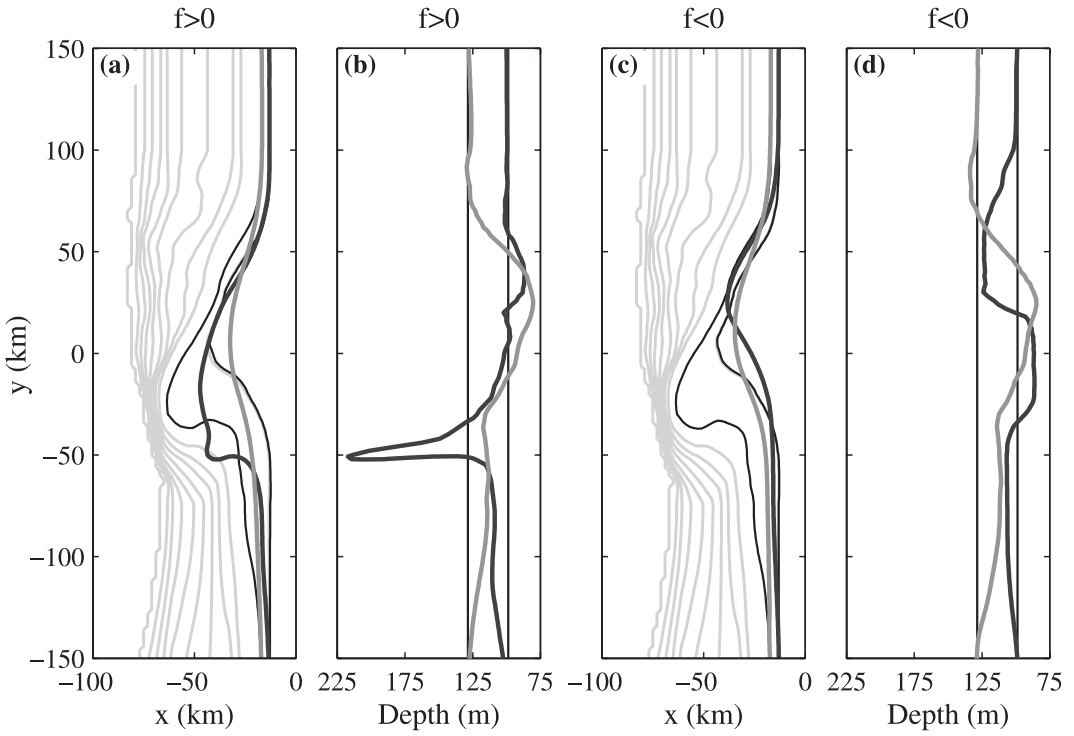

FIG. 9. Path of the streamline following the jet core (day 10): (a) path during Northern Hemisphere runs, (b) bottom depth along path during Northern Hemisphere runs, (c) path during Southern Hemisphere runs, (c) bottom depth along path during Southern Hemisphere runs. The thick dark gray and light gray lines are upwelling and downwelling results, respectively. The thin black lines follow the isobath that the jet cores are centered on along the straight shelf. Thin gray lines contour bathymetry at a 100-m interval.

with the same flow direction, there are substantial differences between the upwelling and downwelling cases, reflecting fundamental differences between the two flow regimes.

The barotropic potential vorticity (PV) is positive everywhere in the Northern Hemisphere runs since f is positive and the relative vorticity is nowhere large enough (Fig. 5) to change the absolute vorticity sign. The terms involving relative vorticity and depth changes that contribute to PV changes along the jet path [Part I, Eq. (3a)] are shown for the Northern Hemisphere upwelling (Fig. 10a) and downwelling (Fig. 10b) runs. Positive derivatives indicate increasing PV due to either shoaling or relative vorticity increasing (becoming less anticyclonic or more cyclonic). As for the standard symmetric bank (Part I), barotropic potential vorticity is not conserved in either the upwelling or downwelling case. Frictional and baroclinic torques are reasons potential vorticity is not conserved. Even though barotropic potential vorticity is not conserved, relative vorticity changes and depth changes partially counter each other in both cases. Because of this tendency (also seen in Part I), the upwelling jet tends to curve back toward its initial isobath while the downwelling jet tends to bend away. This dynamical difference causes the upwelling jet to oscillate about its initial isobath until the pronounced flow separation where isobaths turn sharply, while the downwelling jet bends away from its initial isobath and shoals over the bank.

4. Dynamics

The dynamics controlling upwelling and downwelling circulation over the bank are discussed in this section. Depth-averaged momentum balances for the Northern Hemisphere upwelling and downwelling cases are analyzed. Depth-averaged density balances and vertical velocities also are described.

a. Momentum balance

As in Part I, the lowest-order depth-averaged across-stream momentum balance (not shown) is geostrophic in all cases. This discussion focuses on the depth-averaged alongstream momentum balance (which does not involve Coriolis acceleration).

As in Part I, all terms in the alongstream momentum balance are important over the bank in the upwelling case (Fig. 11). Local acceleration is strongest over the

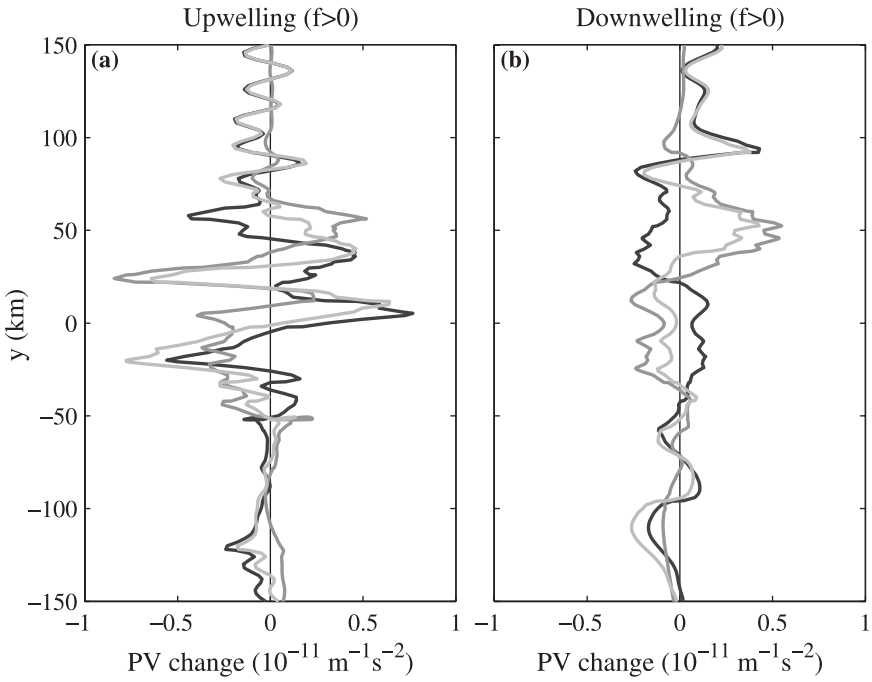

FIG. 10. Changes in barotropic potential vorticity [PV = $(f + \zeta)/h$] along the streamline following the jet core in the Northern Hemisphere (a) upwelling and (b) downwelling cases. The thick light gray, dark gray, and black lines indicate $D(\mathrm{PV})/Dt$, $-(\mathrm{PV}/h)Dh/Dt$, and $(1/h)D\zeta/Dt$, respectively.

bank. The main jet is decelerating along its shoreward side and accelerating along its seaward side. This pattern is associated with the continued offshore movement of the main jet. Advection and alongstream pressure gradients tend to oppose each other. The main jet advects momentum over the bank; this continues extending the high-velocity region. Advection is negative over one part of the northern bank and near the coast on the southern half. The pressure gradient is favorable to southward flow in these regions; there is an adverse pressure gradient along the rest of the main jet path. Surface stress opposes the favorable pressure gradient where currents are reversed. Bottom stress generally opposes surface stress; it is strongest over the bank. The momentum balances over the Heceta Bank complex are qualitatively similar to those over the standard symmetric bank (Part I); the advection field and alongstream pressure gradients have the largest differences.

In the downwelling case, all momentum terms are important over the bank (Fig. 12). Local acceleration is weaker than during upwelling and jet velocities are slower. Bands of acceleration and deceleration are associated with the continued offshore movement of the downwelling jet. Momentum is advected into the slower velocity region over the bank. These slower velocities are advected into the convergence zone at the northern (downstream) edge of the bank. Advection is opposed by an adverse alongstream pressure gradient near the coast over the southern (upstream) bank section and a favorable pressure gradient over the rest of the bank. The symmetric bank results (Part I) share this transition from an adverse pressure gradient upstream to a favorable pressure gradient downstream. As in Part I, the adverse pressure gradient balances wind stress close to the coast. Bottom stress opposes surface stress; it is strong near the coast and along much of the offshore bank edge. The surface stress and bottom stress fields are qualitatively similar to the upwelling case, except where currents oppose winds during upwelling conditions. The advection and pressure gradient fields share less similarity with the upwelling case.

b. Density balance

The density tendency and net advection terms in the depth-averaged density equation [Part I, Eq. (6)] are shown for the Northern Hemisphere upwelling (Fig. 13) and downwelling (Fig. 14) cases. Density is increasing along the upwelling front. The depth-averaged tendency term is largest over bank center. Across-shelf advection associated with the local upwelling circulation leads to density changes over the straight shelf. Both

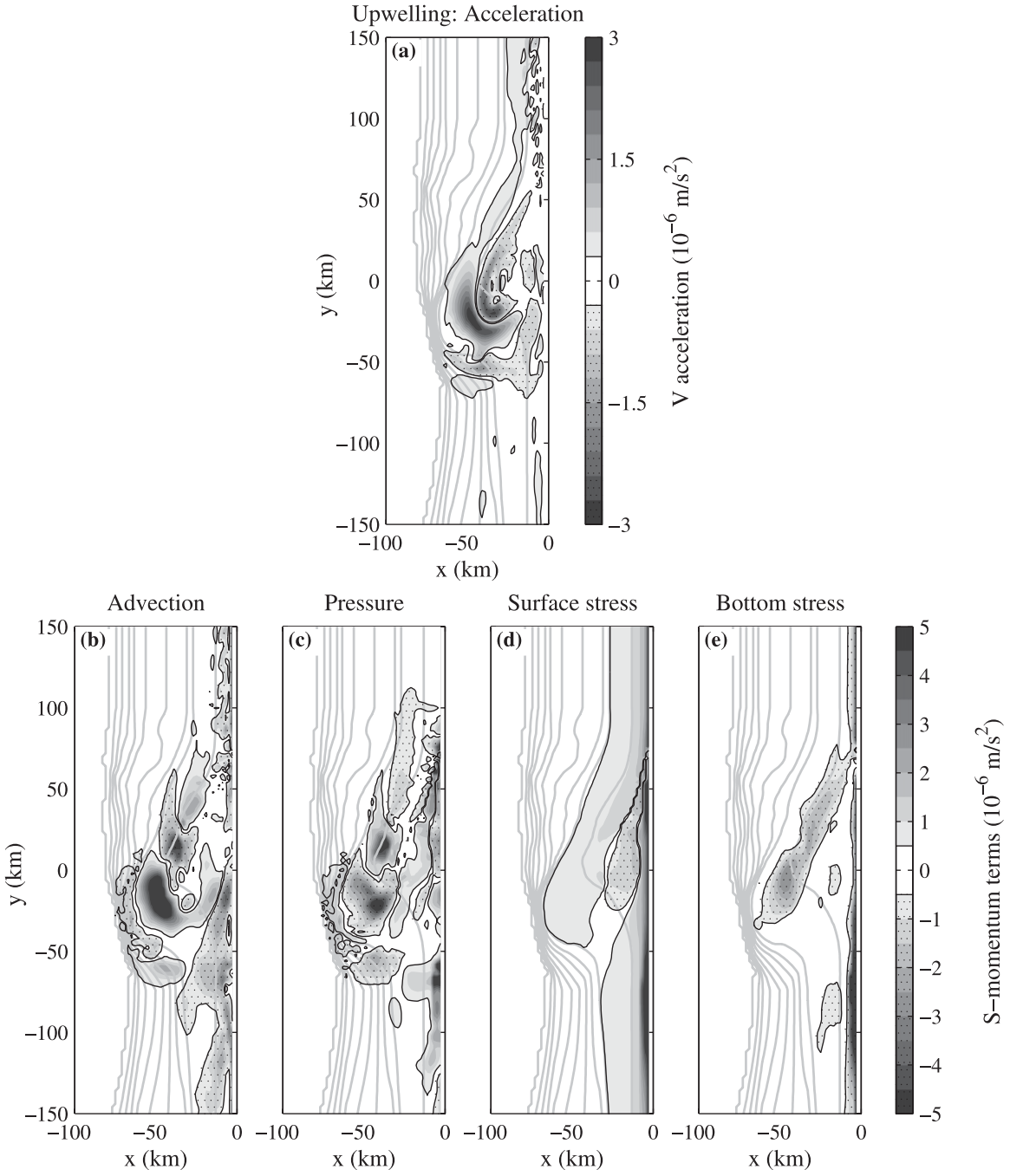

FIG. 11. Depth-averaged alongstream momentum terms for the Northern Hemisphere upwelling run (day 10). The local acceleration is on the left-hand side of the momentum equation and all other terms are on the right-hand side. Positive values indicate a tendency to accelerate flow. Isobaths are shown as in Fig. 4.

across-shelf and alongshelf density advection are important over the bank. During the first days of winds (not shown), alongshelf advection dominates at the northern bank edge. By day 10, across-shelf advection dominates along the upwelling front over the northern section of the bank. Alongshelf advection acts over the upstream half but only dominates along the seaward side of the jet and where the high-velocity jet and dense water tongue are extending farther over the bank. Where flow turns onshore and currents reverse, both across-shelf and alongshelf advection lead to pronounced density increases. There are similarities with

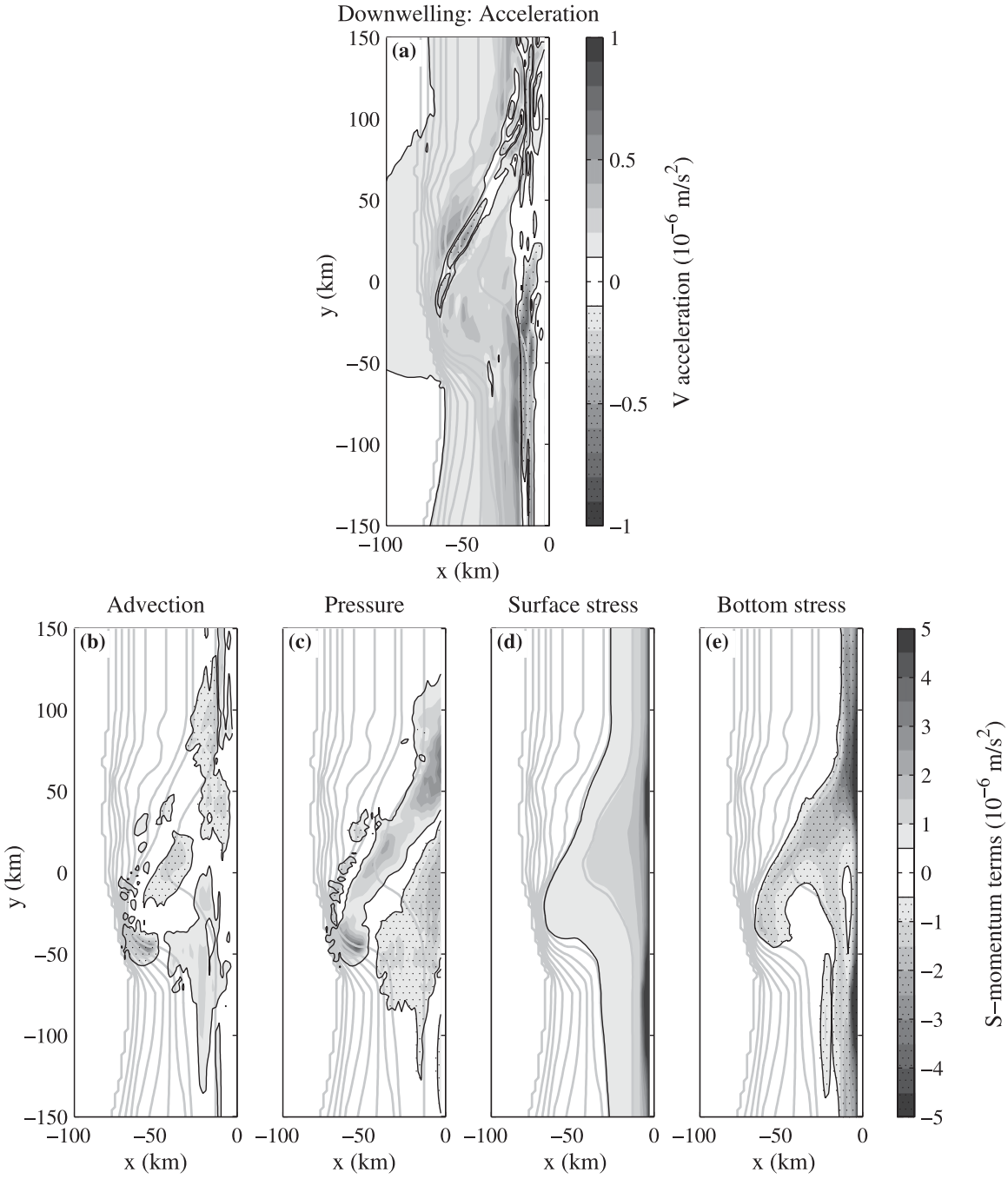

FIG. 12. Depth-averaged alongstream momentum terms for the Northern Hemisphere downwelling run (day 10). The panels are described in the Fig. 11 caption.

the density balances over the symmetric bank (Part I), but bank asymmetry leads to stronger density changes over the southern bank.

The density decrease rates along the downwelling front (Fig. 14) are lower in magnitude than the density increase rates in the upwelling case. Both across-shelf and alongshelf advection are important over the bank. The density tendency is negative over most of the bank. By day 10, across-shelf advection dominates over the southern half and alongshelf advection dominates over the northern (downstream) half. At earlier times (not shown), alongshelf advection dominates over a smaller area near the northern bank edge. The density decreases associated with the local across-shelf

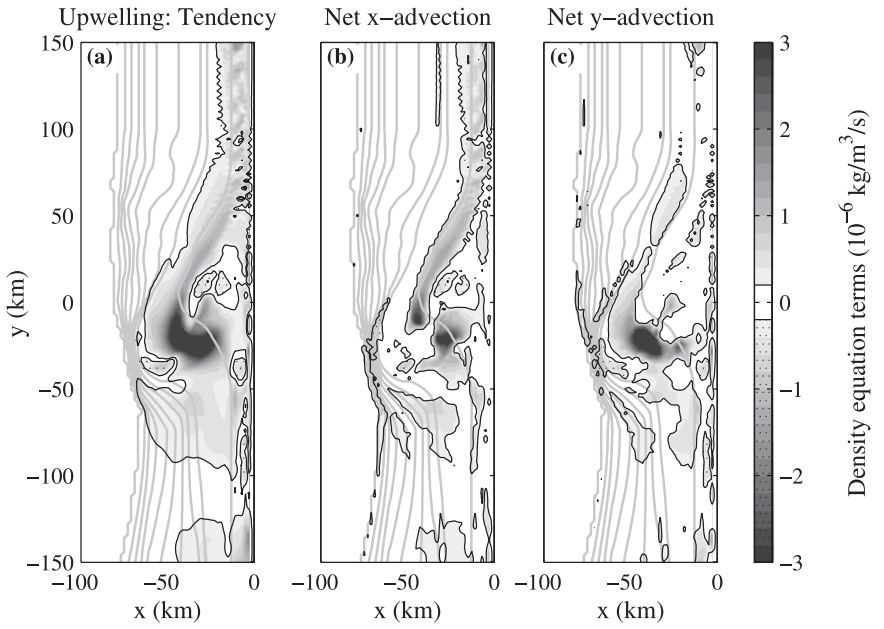

FIG. 13. Depth-averaged density equation terms during the Northern Hemisphere upwelling run (day 10). The tendency term is on the left-hand side of the density equation and the net advection terms are on the right-hand side. Positive values indicate a tendency to increase density. The net *x* and *y* advection terms show only the unbalanced part that effects density change (a large part of the gross advection terms balances partially because of continuity). Isobaths are shown as in Fig. 4.

downwelling circulation are augmented by the offshore jet deflection over the upstream bank half. These density balances are qualitatively similar to the standard symmetric bank results of Part I.

c. Vertical velocity contributions

It is important to identify areas with large vertical velocities and to describe the dynamics creating active upwelling and downwelling zones. As in Part I, contributions to vertical velocities at the top of the bottom boundary layer are discussed, similar to the approach of Kurapov et al. (2005). These contributions include the effects of topographic upwelling and downwelling due to inviscid flow crossing isobaths (w_{topo}) and bottom Ekman pumping created by bottom stress curl (w_{pump}).

There are patches of strong upward and downward velocities shoreward of the 200-m isobath over the bank during upwelling conditions (Fig. 15a). The vertical velocity field is patchier than over the standard symmetric bank studied in Part I. There is strong upwelling at the northern (upstream) bank edge and over the southern (downstream) part of the bank. There also is an upwelling patch between the two strong downwelling patches along the main jet path. Topographic upwelling and downwelling (Fig. 15b) contributes to the strong vertical velocities in these patches; flow shoals where there is topographic upwelling and moves over deeper waters where there is topographic downwelling. The w–w_{topo} field (Fig. 15c) has a band of positive velocity (inshore of the 100-m isobath over the northern bank) and a band of negative velocity (offshore of the 100-m isobath). These bands coincide with the upwelling and downwelling bands that would result if only bottom Ekman pumping were acting (Fig. 15d). This contribution from bottom stress curl adds to the topographic term in some areas and partially counters it in others.

In the downwelling case, there are strong downward velocities (Fig. 16a) near the coast along the straight shelf and along much of the offshore bank edge. There is a patch of active upwelling inshore of the 200-m isobath on the southern (upstream) part of the bank. Comparing the downwelling and upwelling cases indicates there are areas of the bank that experience active upwelling or downwelling in both regimes (e.g., the upwelling patch near the sharply turning 200-m isobath). Large areas of the bank have small vertical velocities in the downwelling case. As in the upwelling case, topographic upwelling and downwelling (Fig. 16b) is the strongest contribution to the vertical velocity field. The w–w_{topo} field (Fig. 16c) reveals bands of downwelling and upwelling that are evident in the Ekman pumping contribution (Fig. 16d). The bottom stress curl partially counters the topographic contribution over most areas of the bank.

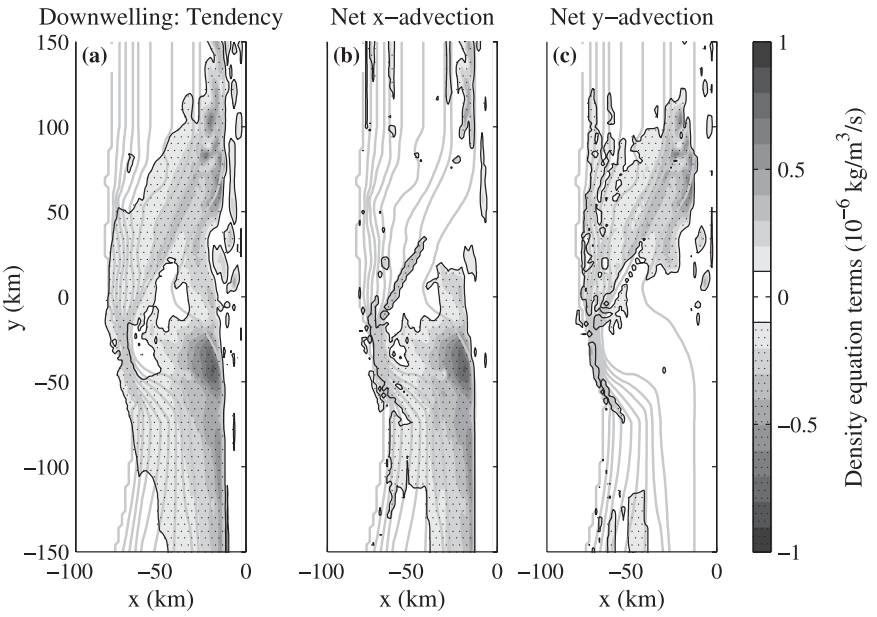

FIG. 14. Depth-averaged density equation terms during the Northern Hemisphere downwelling run (day 10). The panels are described in the Fig. 13 caption; note the color contour range is 3 times smaller than the range in Fig. 13.

5. Summary and conclusions

This part of the study applies the analysis of Part I to the Heceta Bank complex along the Oregon coast. The Heceta Bank complex has similar dimensions to the standard symmetric bank (Part I), but the bank isobaths are oblique and asymmetric (Fig. 1). There are fundamental differences between the upwelling and downwelling dynamics over the symmetric bank. The contrast is more pronounced over the Heceta Bank complex. These runs are forced with steady 0.1-Pa upwelling-favorable (southward for $f > 0$) or downwelling-favorable winds (northward for $f > 0$). Hypothetical Southern Hemisphere cases ($f < 0$) also are analyzed to help discriminate between effects related to bank asymmetry and those linked to differences in upwelling and downwelling dynamics. In all cases, there is significant departure from 2D (without alongshelf variability) wind-driven upwelling circulation over the bank. There is pronounced alongshelf variability in the current and density fields.

The upwelling front and southward baroclinic jet are centered on the 100-m isobath along the straight shelf. The front and jet approximately follow this isobath offshore over the northern part of the bank. The jet separates from the sharply turning isobaths on the southern bank and flows over deeper waters. Flow turns back toward the coast downstream. In this turning region, northward currents flow back onto the bank. The current reversal is connected to the advection of a dense water tongue across the bank. The across-shelf density and baroclinic pressure gradients change sign along the shoreward side of this density tongue; the depth-averaged pressure gradient also changes sign and drives the northward flow. The reversed currents turn again at the bank center and join a secondary southward coastal jet. The secondary coastal jet and corresponding density front are produced by local wind-driven upwelling. The secondary coastal front and jet have been observed over the Heceta Bank complex (e.g., Barth et al. 2005; Kosro 2005). Many areas of the bank show little density change during upwelling conditions. There are two intense upwelling zones: at the upstream bank edge near the coast and on the southern edge in the turning region. These upwelling zones are related to shoaling flow that lifts dense waters onto the bank. In the downwelling case, the density front and northward jet are centered on the 130-m isobath along the straight shelf. The downwelling jet shoals over the bank (to the 80-m isobath) instead of bending around the initial isobath; the jet returns to its initial isobath farther downstream. There is much less offshore deflection than in the upwelling case and currents do not reverse anywhere. The jet is slower and wider over the bank. The water column is well mixed inshore of the downwelling front. The Heceta Bank complex is an area of reduced downwelling. The hypothetical Southern Hemisphere upwelling jet flows in the same direction as the Northern Hemisphere downwelling jet, but there are pronounced

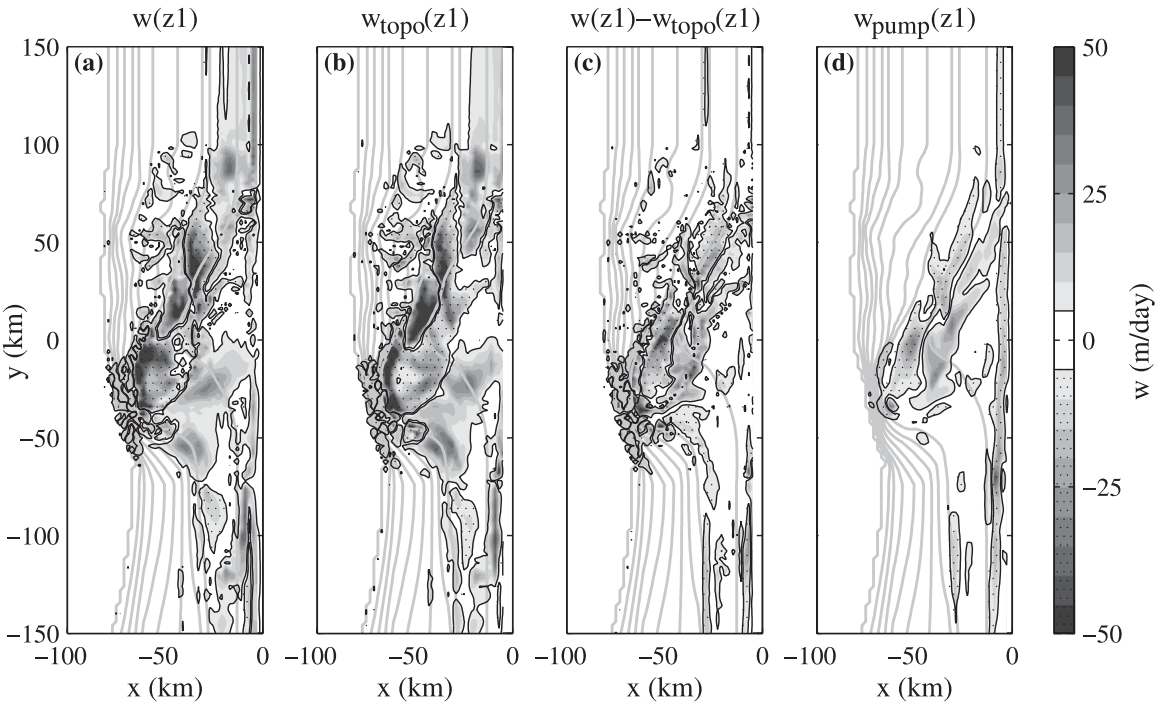

FIG. 15. Vertical velocities at the top of the bottom boundary layer during upwelling (day 10): (a) total vertical velocity, (b) topographic vertical velocity, (c) vertical velocity not due to topographic upwelling or downwelling, and (d) bottom Ekman pumping velocity. Isobaths are shown as in Fig. 4.

differences in the jet paths. The Southern Hemisphere upwelling jet shoals upon separating from isobaths over the southern side of the bank. This jet behaves differently from the Northern Hemisphere upwelling jet because it approaches the tightly turning isobaths from a different direction. The Southern Hemisphere downwelling case is similar to the Northern Hemisphere downwelling case.

Barotropic potential vorticity is not conserved over the Heceta Bank complex during upwelling and downwelling. Nevertheless, depth changes and relative vorticity changes partially counter each other. This tendency produces different consequences of isobath departure for the upwelling and downwelling jets: the upwelling jet tends to bend back toward its initial isobath, while the downwelling jet tends to curve away from its original isobath. Consequently, the Northern Hemisphere upwelling jet oscillates around its original isobath over the northern (upstream) part of the bank. After the flow separation to the south, the upwelling jet curves back toward its initial isobath and returns to this isobath farther downstream. The downwelling jet bends away from its initial isobath and quickly shoals over the southern (upstream) bank section.

Depth-averaged momentum balances are qualitatively similar to Part I. The across-stream momentum balance remains geostrophic over the Heceta Bank complex during upwelling and downwelling conditions. Local acceleration, advection, ageostrophic pressure gradients, surface stress, and bottom stress all are important in the alongstream momentum balance over the bank. There is striking variation in the alongstream momentum balances over different bank sections. The most pronounced differences from Part I are in the advection and pressure gradient terms. Analysis of the depth-averaged density equation indicates that both across-shelf and alongshelf density advection are important over the bank during upwelling and downwelling.

Strong vertical velocities indicate zones of active upwelling and downwelling. There are areas of strong upward and downward velocities over the bank in both the upwelling and downwelling cases. There also are large portions of the bank with little active upwelling or downwelling. Topographic upwelling and downwelling is the largest contribution to vertical velocities over the Heceta Bank complex, but the contribution of bottom Ekman pumping also is evident. The vertical velocity fields are much patchier than for the standard run in Part I. In both the upwelling and downwelling cases, there is an area of upwelling over the southern part of the bank where flow shoals over tightly turning isobaths. There also are areas that have active downwelling in

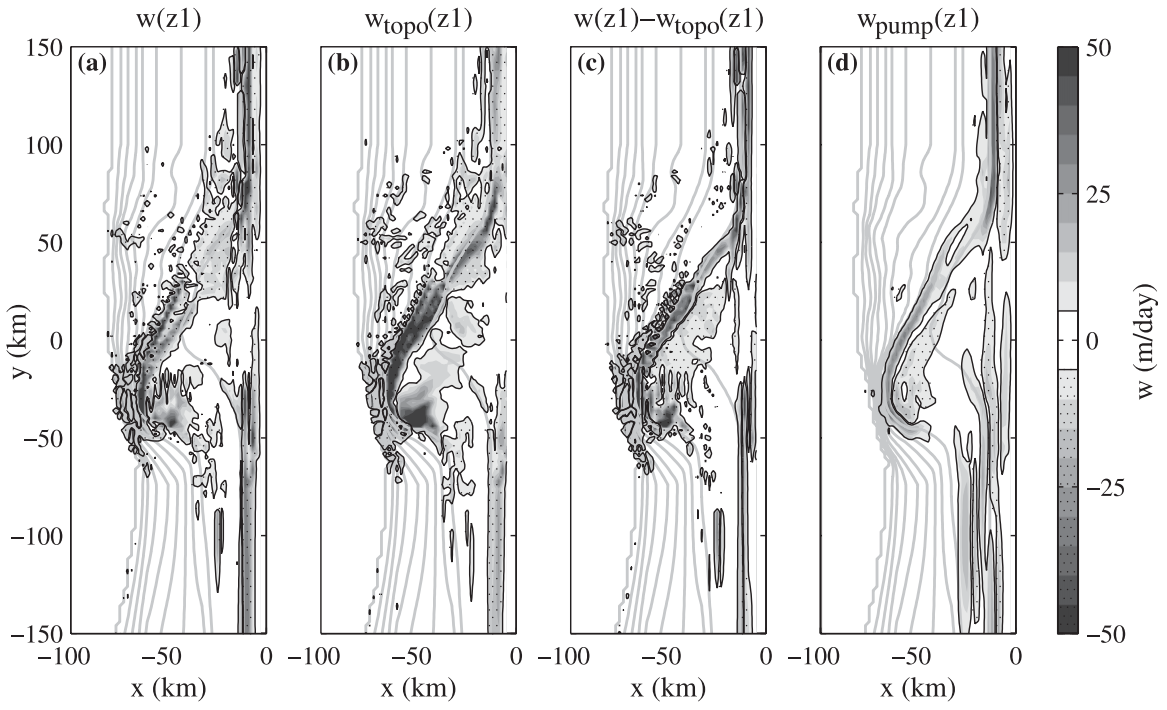

FIG. 16. Vertical velocities at the top of the bottom boundary layer during downwelling (day 10). The panels are described in the Fig. 15 caption.

both upwelling and downwelling cases. These results suggest that parts of the Heceta Bank complex should experience sustained upwelling or downwelling even when winds shift from upwelling favorable to downwelling favorable (or vice versa).

Many of the differences between the upwelling and downwelling regimes over the Heceta Bank complex are anticipated by the symmetric bank results (Part I). The bank is an upwelling center during upwelling conditions and an area of reduced downwelling during downwelling conditions. The upwelling jet follows isobaths offshore over the bank, while the slower downwelling jet shoals over the bank and remains closer to the coast. During upwelling conditions, there are reversed currents over the bank; in contrast, there are no reversed currents during downwelling. Other differences, not anticipated by the standard symmetric bank results, arise because of bank asymmetry and the tightly turning isobaths over the southern part of the bank. The upwelling jet flows over deeper waters over the southern bank; this departure is due to separation from the sharply turning isobaths. This flow separation leads to a larger difference between the upwelling and downwelling jet paths. The bank asymmetry changes results for different flow directions, especially between the Northern Hemisphere and hypothetical Southern Hemisphere upwelling cases. Overall, the results again show the strong differences in shelf flow interactions with topography under upwelling and downwelling conditions.

Acknowledgments. This study is motivated by the observational and modeling efforts undertaken by the Coastal Ocean Advances in Shelf Transport (COAST) project. The research was supported by the National Science Foundation (NSF) as part of the Coastal Ocean Processes (CoOP) program through the COAST project funded by NSF Grant OCE-9907854. Support for manuscript preparation and publishing was provided by University of Connecticut startup funds.

The authors thank two anonymous reviewers for helpful and constructive comments.

REFERENCES

Allen, J. S., and P. A. Newberger, 1998: On symmetric instabilities in oceanic bottom boundary layers. *J. Phys. Oceanogr.,* **28,** 1131–1151.

Barth, J. A., S. D. Pierce, and R. M. Castelao, 2005: Time-dependent, wind-driven flow over a shallow midshelf submarine bank. *J. Geophys. Res.,* **110,** C10S05, doi:10.1029/2004JC002761.

Castelao, R. M., and J. A. Barth, 2006: The relative importance of wind strength and along-shelf bathymetric variations on the separation of a coastal upwelling jet. *J. Phys. Oceanogr.,* **36,** 412–425.

Gan, J., and J. S. Allen, 2005: Modeling upwelling circulation off the Oregon coast. *J. Geophys. Res.,* **110,** C10S07, doi:10.1029/2004JC002692.

Haidvogel, D. B., H. G. Arango, K. Hedstrom, A. Beckmann, P. Malanotte-Rizzoli, and A. F. Shchepetkin, 2000: Model evaluation experiments in the North Atlantic Basin: Simulations in nonlinear terrain-following coordinates. *Dyn. Atmos. Oceans,* **32,** 239–281.

Kosro, P. M., 2005: On the spatial structure of coastal circulation off Newport, Oregon, during spring and summer 2001 in a region of varying shelf width. *J. Geophys. Res.,* **110,** C10S06, doi:10.1029/2004JC002769.

Kurapov, A. L., J. S. Allen, G. D. Egbert, and R. N. Miller, 2005: Modeling bottom mixed layer variability on the mid-Oregon shelf during summer upwelling. *J. Phys. Oceanogr.,* **35,** 1629–1649.

Oke, P. R., J. S. Allen, R. N. Miller, and G. D. Egbert, 2002: A modeling study of the three-dimensional continental shelf circulation off Oregon. Part II: Dynamical analysis. *J. Phys. Oceanogr.,* **32,** 1383–1403.

Shchepetkin, A. F., and J. C. McWilliams, 2005: The regional oceanic modeling system (ROMS): A split-explicit, free-surface, topography-following-coordinate oceanic model. *Ocean Modell.,* **9,** 347–404.

Whitney, M. M., and J. S. Allen, 2009: Coastal wind-driven circulation in the vicinity of a bank. Part I: Modeling flow over idealized symmetric banks. *J. Phys. Oceanogr.,* **39,** 1273–1297.